Volume 1 | Number 1 | Jan 2013 | Pages 1–100

PCCP

Physical Chemistry Chemical Physics
www.rsc.org/pccp

ROYAL SOCIETY OF CHEMISTRY

ROYAL SOCIETY OF CHEMISTRY

www.rsc.org/pccp

Molecular Dynamics Simulations Predict an Accelerated Dissociation of H_2CO_3 at the Air-Water Interface

Mirza Galib[*] and Gabriel Hanna[*]

Department of Chemistry, University of Alberta, Edmonton, Alberta, Canada

E-mail: mgalib@ualberta.ca; gabriel.hanna@ualberta.ca

Abstract

The dissociation and decomposition reactions of carbonic acid (H_2CO_3) in bulk water have been thoroughly studied, but little is known about its reactivity at the air-water interface. Herein, we investigate the dissociation reaction of H_2CO_3 at the air-water interface using ab initio molecular dynamics and metadynamics. Our results indicate that H_2CO_3 (pK_a=3.45) dissociates faster at the water surface than in bulk water, in contrast to recent experiments and simulations which have shown that HNO_3 (pK_a=-1.3) has a lower propensity to dissociate at the water surface than in bulk water. We find that the water surface allows for a more structured solvation environment around H_2CO_3 than in bulk water, which contributes to a decrease in the dissociation energy barrier via a stabilization of the transition state relative to the undissociated acid. Given its decreased kinetic stability at the air-water interface, H_2CO_3 may play an important role in the acidification of atmospheric aerosols and water droplets.

[*]To whom correspondence should be addressed

Introduction

Reactions of acid gases (e.g., SO_2, NO_2, CO_2, etc.) and their associated acids with aqueous aerosols and water droplets are ubiquitous in the atmosphere.[1–4] Mechanistic insight into these reactions is important for understanding the composition and reactivity of other gases in aerosols and water droplets and the role played by such particles in atmospheric pollution and the greenhouse effect.[2,4] Since the first point of contact with a water droplet or aerosol is its surface, a detailed understanding of the reactivity of acid gases and their associated acids at the air-water interface is crucial. In particular, the kinetics and energetics of acid dissociation at the air-water interface are expected to be significantly different than those in bulk water since the intermolecular forces experienced are fundamentally different in interfacial environments than in bulk environments.[5–7] For example, both experimental and computational studies have shown that the dissociation energetics and kinetics of HNO_3 change significantly at the water surface.[5,8,9] More specifically, X-ray photoelectron spectroscopy has shown that the degree of dissociation of HNO_3 decreases by $\sim 20\%$ at the water surface relative to in bulk water.[5] This study was accompanied by ab initio molecular dynamics simulations which found that the solvation environment around HNO_3 at the water surface is more structured than in bulk water, and could thereby stabilize the undissociated HNO_3. Another ab initio molecular dynamics study has shown that HNO_3 remains undissociated at the water surface during a 20 ps long simulation, suggestive of a more stable HNO_3 at the surface and a higher dissociation energy barrier than in the bulk (cf. in bulk, HNO_3 was found to dissociate within 0.5 ps).[8] A classical molecular dynamics study of the hydration structure of NO_3^- has revealed that the hydrogen bond distances between an oxygen of NO_3^- and adjacent water hydrogens increase at the surface compared to in the bulk (1.95 Å vs. 1.87 Å), suggesting that NO_3^- is preferentially stabilized in the bulk than at the surface.[10] Although these results can explain the shift in the equilibrium at the surface favouring HNO_3 over NO_3^-, it is not clear why the dissociation barrier increases at the surface. Hence, further computational studies of the dissociation of atmospherically relevant acids on the surface of water are needed to elucidate the underlying reasons for these changes in dissociation behaviour.

2

In this article, we focus on carbonic acid (H_2CO_3), one of the prevalent acids in the atmosphere, since its reactivity at the air-water interface has been previously studied neither experimentally nor theoretically. In the presence of water, H_2CO_3 can dissociate to form HCO_3^- and H_3O^+ and thereby increase the acidity of its environment. Its pK_a was previously thought to be ~ 6.4, based on electromotive force and conductance measurements.[11–13] However, it was later discovered that this is not the true pK_a, since the earlier experiments had taken into account the equilibrium with CO_2 and H_2O in addition to the dissociation, i.e., $CO_2 + 2H_2O \rightleftharpoons H_2CO_3 + H_2O \rightleftharpoons HCO_3^- + H_3O^+$. The actual pK_a lies in the range of $3.4 - 3.8$,[14–18] indicating that H_2CO_3 is a stronger acid than originally believed and is comparable in acidity to, for example, formic acid ($pK_a \sim 3.8$). Therefore, the impact of H_2CO_3 on the acidity of atmospheric aerosols and water droplets should not be neglected in view of its presence in the upper troposphere (it is formed by the reaction of gaseous CO_2 with water clusters[19] or by the sublimation of solid H_2CO_3[19,20]), especially in light of the increasing CO_2 levels in the atmosphere.

The decomposition of H_2CO_3 into CO_2 in the gas phase and in bulk water has been studied extensively both experimentally[16,19,21–25] and theoretically.[17,18,26–36] In the gas phase, H_2CO_3 has a high decomposition energy barrier of ~ 43.5 kcal/mol,[28] but in the presence of water, the barrier decreases substantially to ~ 15 kcal/mol.[15,24,37] As a result, the lifetime of H_2CO_3 in water is short (~ 300 ns[16]), which has made it difficult for experiments to identify the exact elementary steps of the decomposition mechanism. However, recent theoretical studies have revealed that the decomposition of H_2CO_3 in bulk water (i.e., $H_2CO_3 \rightleftharpoons CO_2 + H_2O$) occurs predominantly via a step-wise mechanism (i.e., dissociation into HCO_3^- and H_3O^+ first, followed by decomposition of HCO_3^- into CO_2 and H_2O), as opposed to both step-wise and concerted mechanisms.[17,38] This is in contrast to the gas phase decomposition, which solely takes place in a concerted fashion via a cyclic transition state.[32] In a recent ab initio metadynamics study of H_2CO_3 decomposition in water clusters,[38] it was found that a mechanistic shift from the concerted to the step-wise pathway takes place when there is a sufficient number of water molecules solvating the H_3O^+. These water molecules stabilize the H_3O^+, which prevents a rapid recombination of the HCO_3^- and H_3O^+

ions and thereby leads to the formation of a stable solvent-separated HCO_3^-/H_3O^+ ion pair, a pre-requisite for the step-wise decomposition to occur.

To gain a microscopic understanding of the reactivity of H_2CO_3 at the surface of a water droplet, we investigated the dissociation of H_2CO_3 at the air-water interface and the solvation environments experienced by the acid and its conjugate base using Car-Parrinello molecular dynamics (CPMD)[39] and metadynamics.[40] The mechanisms and timescales of the dissociation are elucidated and a free energy surface along collective variables (CVs) appropriate for the dissociation at the water surface is constructed. From this, an upper limit on the dissociation free energy barrier is extracted and insight into the differences between reactions at the water surface and in the bulk is gained. Based on our findings, we also propose a reason for why HNO_3 has a higher dissociation barrier at the water surface than in the bulk.

Computational Details

The dissociation of H_2CO_3 at the air-water interface was investigated using CPMD. To construct the water surface, we first added 49 pre-equilibrated water molecules to an 11.4 X 11.4 X 11.4 Å^3 box with periodic boundary conditions in the x and y directions, but not in the z direction (giving rise to ∼5 molecular layers). We note that 5 water layers were also used in a CPMD study of the dissociation of HNO_3 on top of and within a water slab.[9] Then, the box was elongated by 8.5 Å in both the $+z$ and $-z$ directions to create vacuums above and below the water cube, and equilibrated for 10 ps. This approach was previously used to study the interfacial reactivities of HNO_3[5,8,9] and H_2SO_4.[41] Different initial configurations were generated by introducing a cis-trans H_2CO_3 molecule at different positions above the water cube and with different orientations with respect to the water surface. More specifically, we considered two orientations: (i) *Orientation A*− the OH group cis to the carbonyl oxygen pointing toward the surface, and (ii) *Orientation B*− the OH group trans to the carbonyl oxygen pointing toward the surface. The two positions we considered are (i) *Position 1*− H_2CO_3 physisorbed to the water surface (the distance between the hydroxyl

hydrogen of H_2CO_3 and the nearest water oxygen is ~3.5 Å), and (ii) *Position 2*− H_2CO_3 above

the water surface (the distance between the hydroxyl hydrogen of H_2CO_3 and the nearest water

oxygen is ~5.0 Å). Therefore, we generated four types of initial configurations corresponding to all

combinations of orientations and positions (denoted by A1, A2, B1, and B2), as depicted in Figure

1. Using CPMD, each configuration was equilibrated for another picosecond, followed by a 15 ps

production run. This procedure was followed to generate an ensemble of three different trajectories

for each type of initial configuration, in order to validate the reproducibility of our observations. All

simulations were carried out at a temperature of 300 K (with the aid of Nosé-Hoover thermostats),

in order to compare our results to previous results for H_2CO_3 in bulk water at this temperature. The

valence electrons were treated within the DFT formalism using the BLYP functional[42,43] and the

interaction between the core and valence electrons was treated using ultrasoft pseudopotentials.[44]

This functional and these pseudopotentials have yielded sensible results in earlier studies of H_2CO_3

in bulk water and water clusters.[17,18,34,38] A plane wave basis set with a cutoff of 40 Ry was used

to expand the Kohn-Sham orbitals. The fictitious electron mass and the time step were 600 a.u. and

4 a.u., respectively.

The dissociation free energy barriers were calculated using metadynamics with two CVs: the

O(4)-H(5) coordination number in H_2CO_3 (CV_1) and the distance between O(4) and the resulting

H_3O^+ ion (CV_2) (see Figure 2 for the atomic labels). CV_1 has the following form:

$$CV_1 = \frac{1 - (\frac{d}{d_0})^p}{1 - (\frac{d}{d_0})^{p+q}},\tag{1}$$

where d is the instantaneous distance between O(4) and H(5), d_0 is the distance below which the

atoms are considered bonded, and p/q are parameters chosen such that the coordination number

tends to zero beyond d_0. CV_2 has the following form:

$$CV_2 = G_{H_2CO_3} R_{H_3O^+}.\tag{2}$$

In the above equation, $R_{H_3O^+}$ is defined as

$$R_{H_3O^+} = \frac{\sum_{j \in O_w} d_j \exp(\lambda n_j^H)}{\sum_{j \in O_w} \exp(\lambda n_j^H)},$$ (3)

where d_j is the instantaneous distance between O(4) in H_2CO_3 and a particular water oxygen, λ is a constant, and n_j^H is the number of hydrogen atoms bonded to that oxygen atom, defined by

$$n_j^H = \sum_{i \in H_w} \frac{1 - (\frac{d_i}{d_0})^p}{1 - (\frac{d_i}{d_0})^{p+q}},$$ (4)

where d_i is the instantaneous distance between the water oxygen atom and a water hydrogen atom, and p and q are parameters chosen such that n_j^H tends to zero beyond d_0. $G_{H_2CO_3}$ is a cutoff function, which becomes approximately zero when the H_2CO_3 is undissociated and there is no H_3O^+ ion present in the system and becomes approximately one when the dissociation takes place. It is defined as

$$G_{H_2CO_3} = 1 - \frac{1 - (\frac{CV_1}{0.1})^p}{1 - (\frac{CV_1}{0.1})^{p+q}},$$ (5)

where p and q are parameters chosen such that $G_{H_2CO_3}$ tends to zero when CV_1 is greater than 0.1. The details, parameters, and an error estimate associated with the metadynamics simulations are provided in the Supporting Information.

Results and Discussion

The dissociation mechanism for configuration A1 is illustrated in Figure 3, which shows snapshots from key points along a representative CPMD trajectory. As shown in Figure 3, H_2CO_3 first chemisorbs to the surface through two hydrogen bonds, one between a surface water oxygen and a hydroxyl oxygen of H_2CO_3 (i.e., hydrogen bond donor) and the other between a surface water oxygen (i.e., hydrogen bond donor) and the carbonyl oxygen of H_2CO_3. An examination of the trajectories of the distances between the hydroxyl hydrogen and the nearest water oxygen and

the hydroxyl oxygen and the nearest water hydrogen (see Figure 4) indeed shows that H_2CO_3 is not hydrogen bonded at the beginning of the simulation, but forms two hydrogen bonds after $\sim$0.6 ps. After 1 ps, H_2CO_3 undergoes dissociation into HCO_3^- and H_3O^+ according to the same steps as in the bulk: (i) the formation a Zundel-like structure (as manifested by a decrease in the distance between the hydroxyl oxygen and the water oxygen in the top right panel of Figure 3), (ii) the breakage of the O-H bond, (iii) the formation of a contact ion pair ($HCO_3^- \cdots H_3O^+$), and (iv) the hopping of the excess proton of H_3O^+ to a neighbouring water molecule via the Grotthuss mechanism resulting in a solvent-separated ion pair ($HCO_3^- \cdots (H_2O)_n \cdots H_3O^+$). For the remainder of the 15 ps trajectory, a recombination of the ions does not occur, i.e., the system has settled into the stable product well. The above observations are common to the other two trajectories generated for this initial configuration type.

In the case of initial configuration A2, we see in Figure 5 that H_2CO_3 approaches the surface and, at $t \approx 2$ ps, donates the proton from its hydroxyl group to form a hydrogen bond with a surface water oxygen. At $t \approx 3$ ps, the carbonyl oxygen accepts a proton from another surface water oxygen to form another hydrogen bond. Once this hydrogen-bonded complex forms with the surface waters, the dissociation takes place via the same steps and in a similar amount of time as in the case of A1. However, in contrast to the case of A1, the hydrogen-bonded complex forms with two water molecules that are displaced from the surface (see panel 2 in Figure 5). This happens due to the fact that, in the case of A2, H_2CO_3 is further from the surface and, as a result, there are fewer waters in its vicinity to solvate it.

In contrast to initial configuration A1, one hydroxyl group and the carbonyl oxygen of initial configuration B1 point toward the vacuum and, in turn, are not available for hydrogen bonding with the water surface (see Figure 1). Therefore, only the remaining hydroxyl group is available for hydrogen bond formation with the surface. In Figure 6, we see that H_2CO_3 first forms a hydrogen bond by donating the proton from this hydroxyl group to a neighbouring water oxygen and, after 2 ps, a second hydrogen bond with the same hydroxyl oxygen by accepting a proton from a neighbouring water (see panel 2 of Figure 6). We have verified that the other hydroxyl oxygen

does not hydrogen bond with the surface water molecules via integration of the radial distribution function (RDF) between that hydroxyl oxygen and the water hydrogens up to 2.5 Å (see top panel of Figure 7), which yields only 0.20. Over the next 2 ps, the dissociation takes place via the same mechanism as in the case of A1 (see panels 2, 3, and 4 in Figure 6), but more slowly than in the case of A1 (4 ps vs. 1 ps). In the case of initial configuration B2, we see that H_2CO_3 first forms a hydrogen bond by donating the proton from the hydroxyl group to a neighbouring water oxygen in 1 ps and, one picosecond later, a *weak* hydrogen bond by accepting a proton from a nearby water through the other hydroxyl oxygen (see Figure 8). This hydrogen bond was deemed to be weak based on a distance of ~2.0 Å between that hydroxyl oxygen and the nearest water hydrogen (determined from the position of the first peak in the RDF between that hydroxyl oxygen and the water hydrogens in the bottom panel of Figure 7) and integration of this RDF up to the first minimum which yields 0.6. In contrast to initial configuration B1, the hydroxyl oxygen that donates a hydrogen bond to a neighbouring water does not accept another hydrogen bond from another water due to the scarcity of waters in its vicinity at this greater distance from the surface (compare panel 2 of Figure 6 to the left panel of Figure 8). For the remainder of the 15 ps trajectory, B2 remains undissociated, unlike the other initial configurations which undergo rapid dissociations. This was also observed in the other two trajectories generated for this initial configuration type.

The above results reveal that the differences in dissociation times for the various relative orientations and distances of H_2CO_3 to the surface are due to the differences in the hydrogen bonding environments experienced by H_2CO_3, which arise due to the anisotropic nature of the water surface. When H_2CO_3 is in the A orientation, hydrogen bonding between the carbonyl oxygen and the surface speeds up the dissociation compared to H_2CO_3 in the B orientation (where the carbonyl oxygen points toward the vacuum and, hence, cannot form a hydrogen bond with the surface). This suggests that hydrogen bond formation between the carbonyl oxygen and water stabilizes (1) the transition state more than the undissociated acid, thereby decreasing the barrier, and (2) the HCO_3^-, thereby facilitating the departure of the H_3O^+ from the HCO_3^-. In the case of configuration B2, H_2CO_3 is not seen to undergo dissociation during the 15 ps trajectories since it forms

8

only one strong hydrogen bond with a nearby water, which does not reduce the energy barrier sufficiently to observe dissociation on the timescale of the simulations.

The formation of the stable solvent-separated ion pair (i.e., the dissociation of H_2CO_3 into HCO_3^- and H_3O^+) observed for the A1, A2, and B1 configurations in our short CPMD runs is significant in several respects. First, our results strongly suggest that the dissociation of H_2CO_3 at the water surface has a substantially lower energy barrier than in bulk water. Previous theoretical studies have found an energy barrier of ~ 9.5 kcal/mol for the dissociation of H_2CO_3 in bulk water.[17,18] In these studies, metadynamics was used to compute the bulk barrier ($\sim 16\, k_b T$ at 300 K), since the dissociation is either rarely or not observed in unbiased CPMD runs that are tens of picoseconds long. Similarly, since configuration B2 did not dissociate within a 15 ps CPMD trajectory, we used metadynamics to calculate the dissociation barrier (see Figure 9 for snapshots of the dissociation mechanism along a representative metadynamics trajectory). Figure 10 shows the dissociation free energy profile. The wells seen in the inset of this figure at $\{CV_1 \approx 0.75\text{-}0.90,$ $CV_2 \approx 0\}$, $\{CV_1 \approx 0.45\text{-}0.55, CV_2 \approx 0\}$, and $\{CV_1 \approx 0.25, CV_2 \approx 0\}$ correspond to the reactant, Zundel-like structure, and contact ion pair, respectively, whereas the well at $\{CV_1 \approx 0, CV_2 \approx 10\}$ corresponds to the solvent-separated ion pair. Based on this profile, the dissociation free energy barrier is 5.0 kcal/mol ± 1.1 kcal/mol ($\sim 8.5\, k_b T$), which constitutes the upper bound of the dissociation barriers encountered in this study. Therefore, the dissociation of H_2CO_3 at the surface of an aqueous particle is expected to be orders of magnitude faster than in the bulk. Second, our results suggest that the concerted decomposition pathway is highly unlikely at the water surface. After the H_3O^+ ion forms at the surface, it diffuses into the bulk and becomes fully solvated there. This allows for the formation of a stable solvent-separated ion pair, despite the fact that the HCO_3^- at the surface is not fully solvated. This is consistent with our recent finding that hydrogen bond formation with the carbonyl oxygen is not a pre-requisite for a step-wise decomposition to occur in bulk water, but rather the full solvation of the H_3O^+ ion, which inhibits the recombination of the ion pair and thereby precludes the concerted pathway.[38] Therefore, we expect H_2CO_3 to decompose via a step-wise pathway at the water surface, but this remains to be confirmed.

The (at least) 4.5 kcal/mol decrease in the dissociation energy barrier in going from the bulk to the surface may happen for one or both of the following reasons: (1) the reactant destabilizes relative to the transition state, and/or (2) the transition state stabilizes relative to the reactant. To gain insight into exactly what causes the accelerated dissociation at the water surface, we must first consider the solvation environment around H_2CO_3. Unlike in bulk water, all of the oxygens and hydrogens in H_2CO_3 cannot be implicated in hydrogen bonds at the surface. However, H_2CO_3 can form hydrogen-bonded complexes with at least two water molecules, as shown earlier. Figure 11 shows the H_2CO_3 carbon−water oxygen RDFs for configurations A2, B1, and B2. These RDFs were calculated based on trajectory data from the start of the production run until the time of dissociation.[45] Overall, they show that the water molecules are well-structured around the H_2CO_3 molecule, even up to the third solvation shell. This should be contrasted with the bulk, where second and third hydration shells cannot be resolved (i.e., the water molecules beyond the first hydration shell are randomly arranged).[34] As mentioned earlier, a structured solvation environment around HNO_3 at the water surface was observed in the ab initio molecular dynamics study of Lewis et al.,[5] but based only on a more structured first peak in the HNO_3 oxygen to water oxygen RDF (as compared to the bulk). In the case of A2, the first peak is centred at $\sim$3.4 Å, which when integrated gives ~ 2, indicating that H_2CO_3 forms a hydrogen-bonded complex with two water molecules. Beyond this first hydration shell, the RDF becomes zero between $\sim 4 - 4.5$ Å due to the fact that, since H_2CO_3 is further from the surface, two water molecules migrate away from the surface to form a hydrogen-bonded complex with the H_2CO_3, leaving a gap between them and the remaining water molecules. Integration of the second and third hydration shells reveals that they each contain three water molecules. In the case of B1, the first peak is centred at $\sim$3.4 Å, which when integrated out to 4 Å reveals that two water molecules are found in this range. However, unlike in the case of A2, there is a shoulder at ~ 3.6 Å since the two hydrogen bonds accepted and donated by the hydroxyl oxygens in H_2CO_3 are not of equal length. In addition, the RDF never becomes zero since, in this case, H_2CO_3 forms a hydrogen-bonded complex with two water molecules closer to the surface than in the case of A2. The second and third hydration shells contain two and one

water molecules, respectively. In the case of B2, the first peak is centred at $\sim$3.4 Å, which when integrated reveals that one water molecule is found in this range. Therefore, unlike A2 and B1, H_2CO_3 is hydrogen-bonded primarily to one water molecule. Like B1, integration of the second and third hydration shells reveals that they contain two and one water molecules, respectively. We also examined the H_2CO_3 oxygen$-$water oxygen and H_2CO_3 hydrogen$-$water oxygen distances to gain insight into the hydrogen bond forming and breaking dynamics for configuration B2 (see Figure 12). For the duration of the 15 ps simulation, these distances do not exceed 2.8 and 1.5 Å, respectively, indicating that the hydrogen bond remains intact. In contrast, in the bulk, the hydrogen bond breaks a few times during the course of a 14 ps simulation (yielding an average hydrogen bond lifetime of several picoseconds).[34] This suggests that the average lifetime at the water surface is longer than in the bulk.

Based on the information in these RDFs and the assumption that the reactant and transition state experience similar solvation environments, we propose that the second reason (mentioned above) is responsible for the decrease in the dissociation energy barrier. Although we did not directly probe the solvation structure of the transition state, the transition state is also expected to experience a structured solvation environment since both H_2CO_3 and HCO_3^- experience such an environment (based on inspections of Figures 13 and 14 for the H_2CO_3 hydroxyl hydrogen$-$water oxygen RDFs for configurations A2, B1, and B2 and the HCO_3^- oxygen$-$water hydrogen RDFs for configurations A1, A2, and B1, respectively). Now, since the transition state is more polar than the reactant, it is expected to be more stabilized than the reactant in this structured solvation environment (due to more favourable electrostatic interactions), giving rise to the decrease in the dissociation barrier. The question is then why does this not happen in the case of HNO_3 at the water surface? As mentioned earlier, the propensity of HNO_3 to dissociate dramatically decreases at the water surface compared to in bulk water.[5,8,9] Although the solvation environment of HNO_3 is more structured at the water surface compared to in the bulk,[5] it is not as well-structured as that of H_2CO_3 and HCO_3^-. Hence, the contribution to the relative stabilization of the transition state is not as large in the case of the HNO_3 dissociation as in the case of H_2CO_3 dissociation. This

combined with the fact that there is a strong electrostatic interaction between NO_3^- and H_3O^+ at the water surface compared to in the bulk, means that more energy has to be put in to separate these ions. Therefore, it is reasonable to expect that the transition state of the HNO_3 dissociation will be significantly higher in energy than in the bulk. It should be noted that in the case of HCO_3^-, this interaction is not as strong due to its smaller charge density.

Concluding Remarks

In summary, we have found that the dissociation energy barrier of H_2CO_3 is substantially reduced at the air-water interface compared to that in bulk water (a few to $\sim 8.5\,k_bT$ at the surface compared to $\sim 16\,k_bT$ in the bulk), based on ab initio molecular dynamics and metadynamics simulations of H_2CO_3 on and near the surface of a slab of water molecules. This could mean that the role played by H_2CO_3 in the acidification of atmospheric aerosols and water droplets may be more important than originally thought. Based on our findings, we proposed that this reduction is due to an enhanced solvation of the transition state (relative to the undissociated acid), owing to the higher structure of interfacial water molecules than bulk ones. This is in stark contrast to HNO_3, whose propensity to dissociate is substantially weaker at the surface of water relative to in the bulk. Our results suggest that the solvation environment of H_2CO_3 is more structured than that of HNO_3 at the water surface, which leads to a higher relative stabilization of the transition state in the case of the H_2CO_3 dissociation. In addition, there is a weaker electrostatic interaction between HCO_3^- and H_3O^+ than between NO_3^- and H_3O^+ at the water surface compared to in the bulk, which means that more energy has to be put in to separate the NO_3^- and H_3O^+ ions. These reasons combined imply that HNO_3 is kinetically more stable at the water surface compared to in the bulk. Overall, these findings give general insight into the kinetic stability of protic acids at the air-water interface.

Supporting Information Available

Details and parameter values for the metadynamics simulations.

Acknowledgement

References

(1) Ravishankara, A. R. Heterogeneous and Multiphase Chemistry in the Troposphere. *Science* **1997**, *276*, 1058.

(2) Tarbuck, T. L.; Richmond, G. L. Adsorption and Reaction of CO_2 and SO_2 at a Water Surface. *J. Am. Chem. Soc.* **2006**, *128*, 3256–3267.

(3) Vaida, V. Perspective: Water Cluster Mediated Atmospheric Chemistry. *J. Chem. Phys.* **2011**, *135*, 020901.

(4) Kolb, C. E. et al. An Overview of Current Issues in the Uptake of Atmospheric Trace Gases by Aerosols and Clouds. *Atmos. Chem. Phys.* **2010**, *10*, 10561.

(5) Lewis, T.; Winter, B.; Stern, A. C.; Baer, M. D.; Mundy, C. J.; Tobias, D. J.; Hemminger, J. C. Does Nitric Acid Dissociate at the Aqueous Solution Surface? *J. Phys. Chem. C* **2011**, *115*, 21183–21190.

(6) Blower, P. G.; Shamay, E.; Kringle, L.; Ota, S. T.; Richmond, G. L. Surface Behavior of Malonic Acid Adsorption at the Air/Water Interface. *J. Phys. Chem. A* **2013**, *117*, 2529–2542.

(7) Blower, P. G.; Ota, S. T.; Valley, N. A.; Wood, S. R.; Richmond, G. L. Sink or Surf: Atmospheric Implications for Succinic Acid at Aqueous Surfaces. *J. Phys. Chem. A* **2013**, *117*, 7887–7903.

(8) Shamay, E. S.; Buch, V.; Parrinello, M.; Richmond, G. L. At the Water's Edge: Nitric Acid as a Weak Acid. *J. Am. Chem. Soc.* **2007**, *129*, 12910–12911.

(9) Wang, S.; Bianco, R.; Hynes, J. T. Depth-Dependent Dissociation of Nitric Acid at an Aqueous Surface: Car-Parrinello Molecular Dynamics. *J. Phys. Chem. A* **2009**, *113*, 1295–1307.

(10) Miller, Y.; Thomas, J. L.; Kemp, D. D.; Finlayson-Pitts, B. J.; Gordon, M. S.; Tobias, D. J.; Gerber, R. B. Structure of Large Nitrate−Water Clusters at Ambient Temperatures: Simulations with Effective Fragment Potentials and Force Fields with Implications for Atmospheric Chemistry. *J. Phys. Chem. A* **2009**, *113*, 12805–12814.

(11) Harned, H. S.; Davis, R. The Ionization Constant of Carbonic Acid in Water and the Solubility of Carbon Dioxide in Water and Aqueous Salt Solutions from 0 to 50°. *J. Am. Chem. Soc.* **1943**, *65*, 2030–2037.

(12) Shedlovsky, T.; MacInnes, D. A. The First Ionization Constant of Carbonic Acid, 0 to 38°, from Conductance Measurements. *J. Am. Chem. Soc.* **1935**, *57*, 1705–1710.

(13) MacInnes, D. A.; Belcher, D. The Thermodynamic Ionization Constants of Carbonic Acid. *J. Am. Chem. Soc.* **1933**, *55*, 2630–2646.

(14) Wissbrun, K. F.; French, D. M.; Patterson, A. The True Ionization Constant of Carbonic Acid in Aqueous Solution from 5 to 45°. *J. Phys. Chem.* **1954**, *58*, 693–695.

(15) Soli, A. L.; Byrne, R. H. CO_2 System Hydration and Dehydration Kinetics and the Equilibrium CO_2/H_2CO_3 Ratio in Aqueous NaCl Solution. *Mar. Chem.* **2002**, *78*, 65–73.

(16) Adamczyk, K.; Prémont-Schwarz, M.; Pines, D.; Pines, E.; Nibbering, E. T. J. Real-Time Observation of Carbonic Acid Formation in Aqueous Solution. *Science* **2009**, *326*, 1690–1694.

(17) Stirling, A.; Papai, I. H_2CO_3 Forms via HCO_3^- in Water. *J. Phys. Chem. B* **2010**, *114(50)*, 16854–16859.

(18) Galib, M.; Hanna, G. Mechanistic Insights into the Dissociation and Decomposition of Carbonic Acid in Water via the Hydroxide Route: an Ab Initio Metadynamics Study. *J. Phys. Chem. B* **2011**, *115*, 15024–15035.

(19) Hage, W.; Liedl, K. R.; Hallbrucker, A.; Mayer, E. Carbonic Acid in the Gas Phase and its Astrophysical Relevance. *Science* **1998**, *279*, 1332–1335.

(20) Bernard, J.; Seidl, M.; Mayer, E.; Loerting, T. Formation and Stability of Bulk Carbonic Acid (H_2CO_3) by Protonation of Tropospheric Calcite. *ChemPhysChem* **2012**, *13*, 3087–3091.

(21) Terlouw, J. K.; Lebrilla, C. B.; Schwarz, H. Thermolysis of NH_4HCO_3 − A Simple Route to the Formation of Free Carbonic Acid (H_2CO_3) in the Gas Phase. *Angew. Chem. Int. Ed. Engl.* **1987**, *26*, 354–355.

(22) Ludwig, R.; Kornath, A. In Spite of the Chemist's Belief: Carbonic Acid is Surprisingly Stable. *Angew. Chem. Int. Ed. Engl.* **2000**, *39*, 1421–1423.

(23) Mori, T.; Suma, K.; Sumiyoshi, Y.; Endo, Y. Spectroscopic Detection of Isolated Carbonic Acid. *J. Chem. Phys.* **2009**, *130*, 204308.

(24) Wang, X.; Conway, W.; Burns, R.; McCann, N.; Maeder, M. Comprehensive Study of the Hydration and Dehydration Reactions of Carbon Dioxide in Aqueous Solution. *J. Phys. Chem. A* **2010**, *114*, 1734–1740.

(25) Mori, T.; Suma, K.; Sumiyoshi, Y.; Endo, Y. Spectroscopic Detection of Most Stable Carbonic Acid, cis-cis H_2CO_3. *J. Chem. Phys.* **2011**, *134*, 044319.

(26) Wight, C. A.; Boldyrev, A. I. Potential Energy Surface and Vibrational Frequencies of Carbonic Acid. *J. Phys. Chem.* **1995**, *99*, 12125–12130.

(27) Nguyen, M. T.; Raspoet, G.; Vanquickenborne, L. G. How Many Water Molecules Are Actively Involved in the Neutral Hydration of Carbon Dioxide? *J. Phys. Chem. A* **1997**, *101(40)*, 7379–7388.

(28) Loerting, T.; Tautermann, C.; Kroemer, R. T.; Kohl, I.; Hallbrucker, A.; Mayer, E.; Liedl, K. R. On the Surprising Kinetic Stability of Carbonic Acid (H_2CO_3). *Angew. Chem. Int. Ed. Engl.* **2000**, *39*, 891–894.

(29) Tautermann, C. S.; Voegele, A. F.; Loerting, T.; Kohl, I.; Hallbrucker, A.; Mayer, E.; Liedl, K. R. Towards the Experimental Decomposition Rate of Carbonic Acid (H_2CO_3) in Aqueous Solution. *Chem.-A Eur. J.* **2002**, *8*, 66–73.

(30) Tossell, J. A. Boric Acid, Carbonic Acid, and N-Containing Oxyacids in Aqueous Solution: Ab Initio Studies of Structure, pKa, NMR Shifts, and Isotopic Fractionations. *Geochimica et Cosmochimica Acta.* **2005**, *69*, 5647–5658.

(31) Leung, K.; Nielsen, I. M. B.; Kurtz, I. Ab Initio Molecular Dynamics Study of Carbon Dioxide and Bicarbonate Hydration and the Nucleophilic Attack of Hydroxide on CO_2. *J. Phys. Chem. B* **2007**, *111*, 4453–4459.

(32) Kumar, P. P.; Kalinichev, A. G.; Kirkpatrick, R. J. Dissociation of Carbonic Acid: Gas Phase Energetics and Mechanism from Ab Initio Metadynamics Simulations. *J. Chem. Phys.* **2007**, *126*, 204315.

(33) Nguyen, M. T.; Matus, M. H.; Jackson, V. E.; Ngan, V. T.; Rustad, J. R.; Dixon, D. A. Mechanism of the Hydration of Carbon Dioxide: Direct Participation of H_2O versus Microsolvation. *J. Phys. Chem. A* **2008**, *112*, 10386–10398.

(34) Kumar, P. P.; Kalinichev, A. G.; Kirkpatrick, R. J. Hydrogen-Bonding Structure and Dynamics of Aqueous Carbonate Species from Car-Parrinello Molecular Dynamics Simulations. *J. Phys. Chem. B* **2009**, *113*, 794–802.

(35) Liu, X.; Lu, X.; Wang, R.; Zhou, H. In Silico Calculation of Acidity Constants of Carbonic Acid Conformers. *J. Phys. Chem. A* **2010**, *114(49)*, 12914–12917.

(36) Stirling, A. HCO_3^--Formation from CO_2 at High pH: Ab Initio Molecular Dynamics Study. *J. Phys. Chem. B* **2011**, *115*, 14683–14687.

(37) Gibbons, B. H.; Edsall, J. T. Rate of Hydration of Carbon Dioxide and Dehydration of Carbonic Acid at 25°. *J. Biol. Chem.* **1963**, *238*, 3502.

(38) Galib, M.; Hanna, G. The Role of Hydrogen Bonding in the Decomposition of H_2CO_3 in Water: Mechanistic Insights from Ab Initio Metadynamics Studies of Aqueous Clusters. *J. Phys. Chem. B* **2014**, *118*, 5983–5993.

(39) Car, R.; Parrinello, M. Unified Approach for Molecular Dynamics and Density-Functional Theory. *Phys. Rev. Lett.* **1985**, *55*, 2471–2474.

(40) Laio, A.; Parrinello, M. Escaping Free-energy Minima. *Proc. Natl. Acad. Sci. USA* **2002**, *99*, 12562.

(41) Hammerich, A. D.; Finlayson-Pitts, B. J.; Gerber, R. B. NOx Reactions on Aqueous Surfaces with Gaseous HCl: Formation of a Potential Precursor to Atmospheric Cl Atoms. *J. Phys. Chem. Letters* **2012**, *3*, 3405–3410.

(42) Becke, A. D. Density-Functional Exchange-Energy Approximation with Correct Asymptotic Behavior. *Phys. Rev. A* **1988**, *38(6)*, 3098–3100.

(43) Lee, C.; Yang, W.; Parr, R. G. Development of the Colle-Salvetti Correlation-Energy Formula into a Functional of the Electron Density. *Phys. Rev. B* **1988**, *37(2)*, 785–789.

(44) Vanderbilt, D. Soft Self-Consistent Pseudopotentials in a Generalized Eigenvalue Formalism. *Phys. Rev. B* **1990**, *41(11)*, 7892–7895.

(45) Since the simulation box was $11.4 \times 11.4 \times 28.4$ Å^3 with periodic boundary conditions in the *x* and *y* directions, the maximum meaningful distance for the RDF is approximately $\sqrt{[(11.4/2)^2 + (11.4/2)^2]} = 8.06$ Å. Therefore, all RDFs were truncated at this distance.
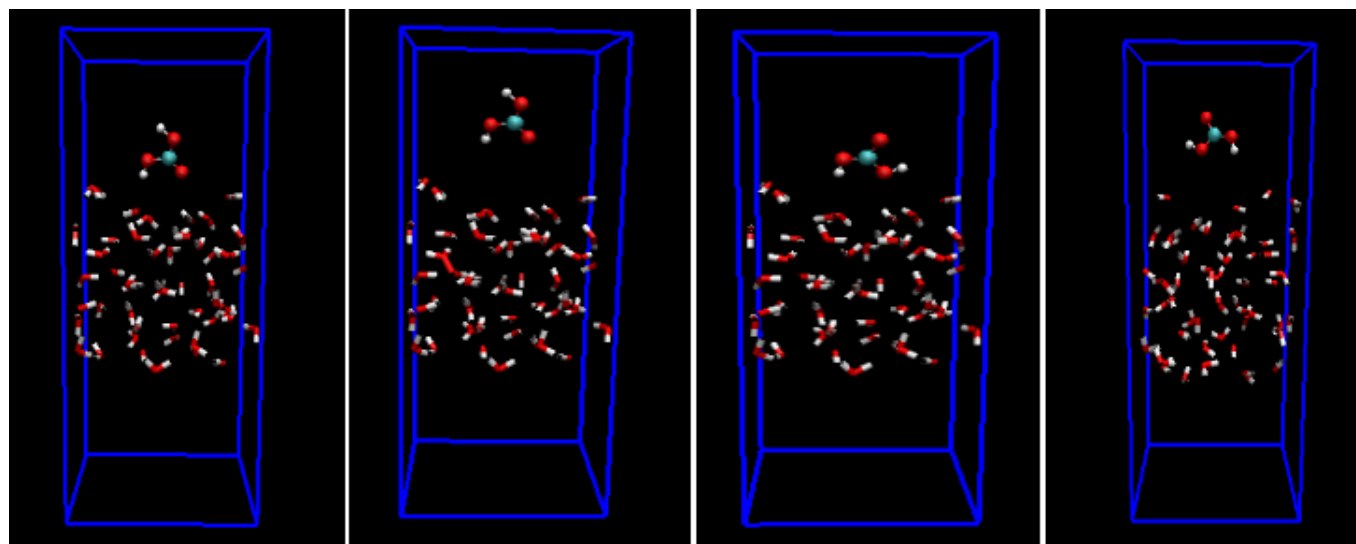
Figure 1: Snapshots of the various initial configurations used in our simulations, each containing one H_2CO_3 on the surface of a water slab. From left to right: 1. H_2CO_3 near the surface, with the carbonyl oxygen pointing toward the surface (configuration A1). 2. H_2CO_3 at a height of 5.0 Å from the surface, with the car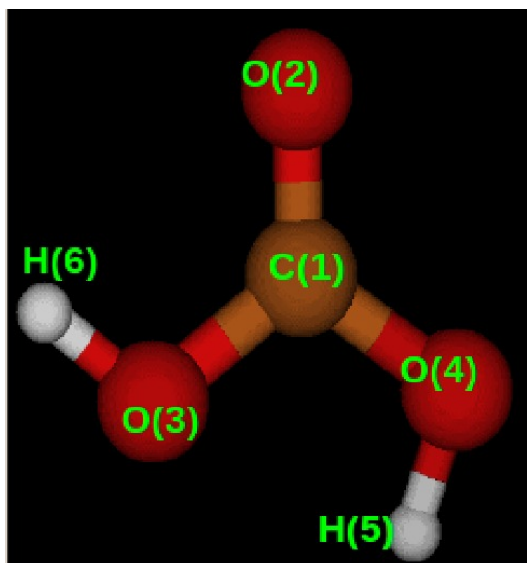bonyl oxygen pointing toward the surface (configuration A2). 3. H_2CO_3 near the surface, with the carbonyl oxygen pointing toward the vacuum (configuration B1). 4. H_2CO_3 at a height of 5.0 Å from the surface, with the carbonyl oxygen pointing toward the vacuum (configuration B2).

Figure 2: The atomic labels used in defining the metadynamics collective variables.
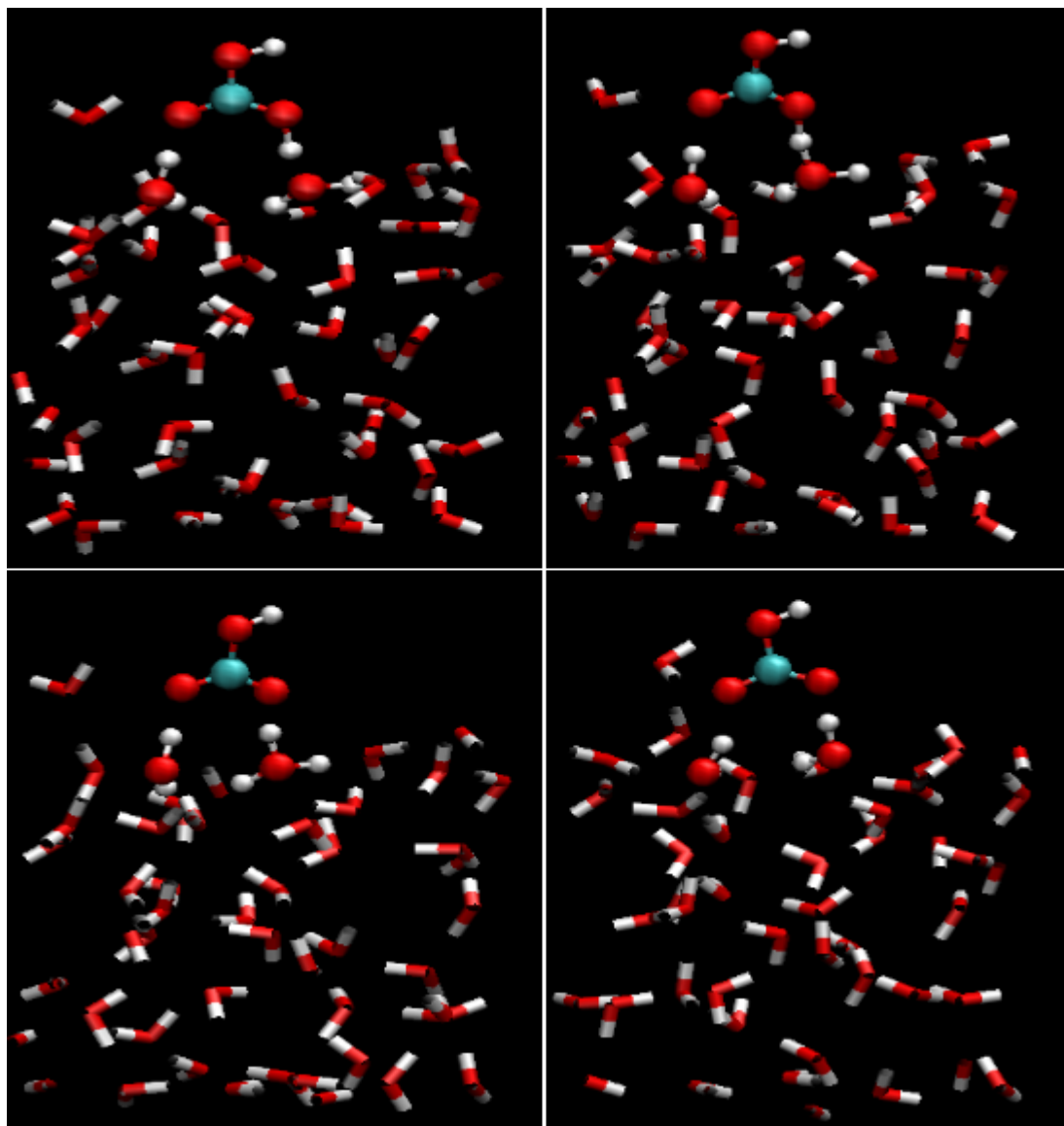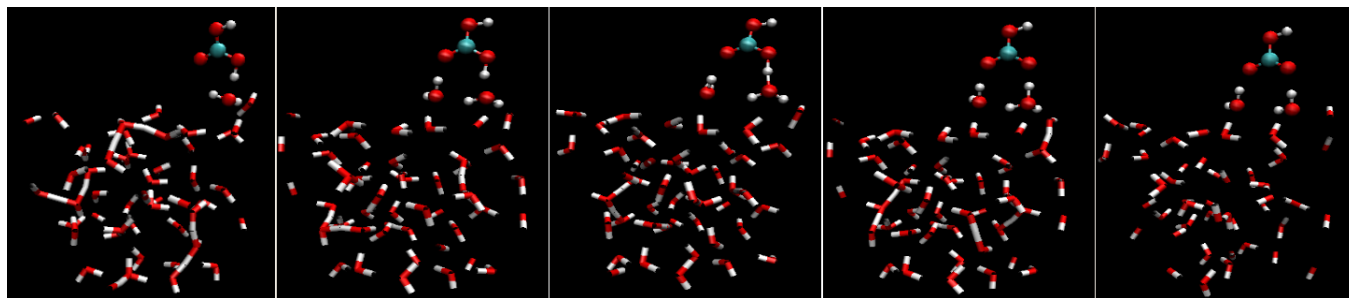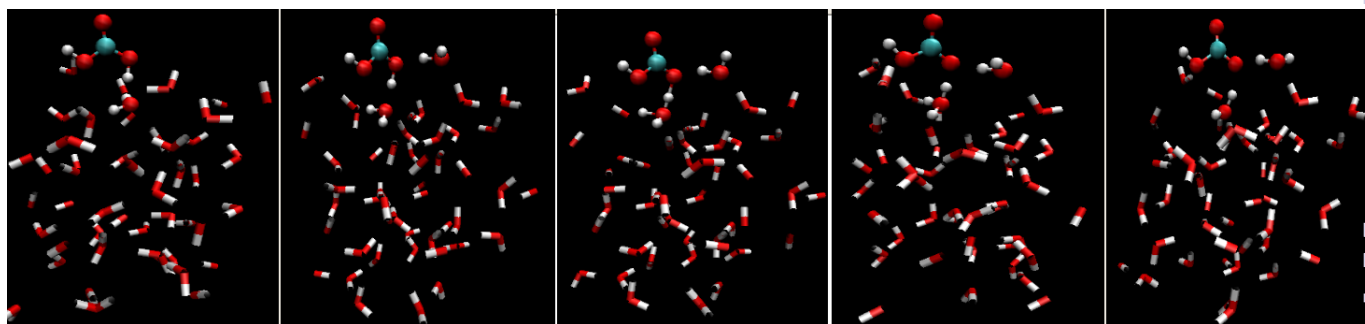
Figure 3: Snapshots of the dissociation of H_2CO_3 from a representative CPMD trajectory starting in configuration A1. Top left: Hydrogen bond formation between H_2CO_3 and two adjacent water molecules ($t \approx 0.5$ ps). Top right: Formation of a Zundel-like structure ($t \approx 0.8$ ps). Bottom left: Formation of a contact ion pair ($t \approx 1.0$ ps). Bottom right: Complete dissociation takes place yielding a solvent-separated ion pair ($t \approx 1.1$ ps).
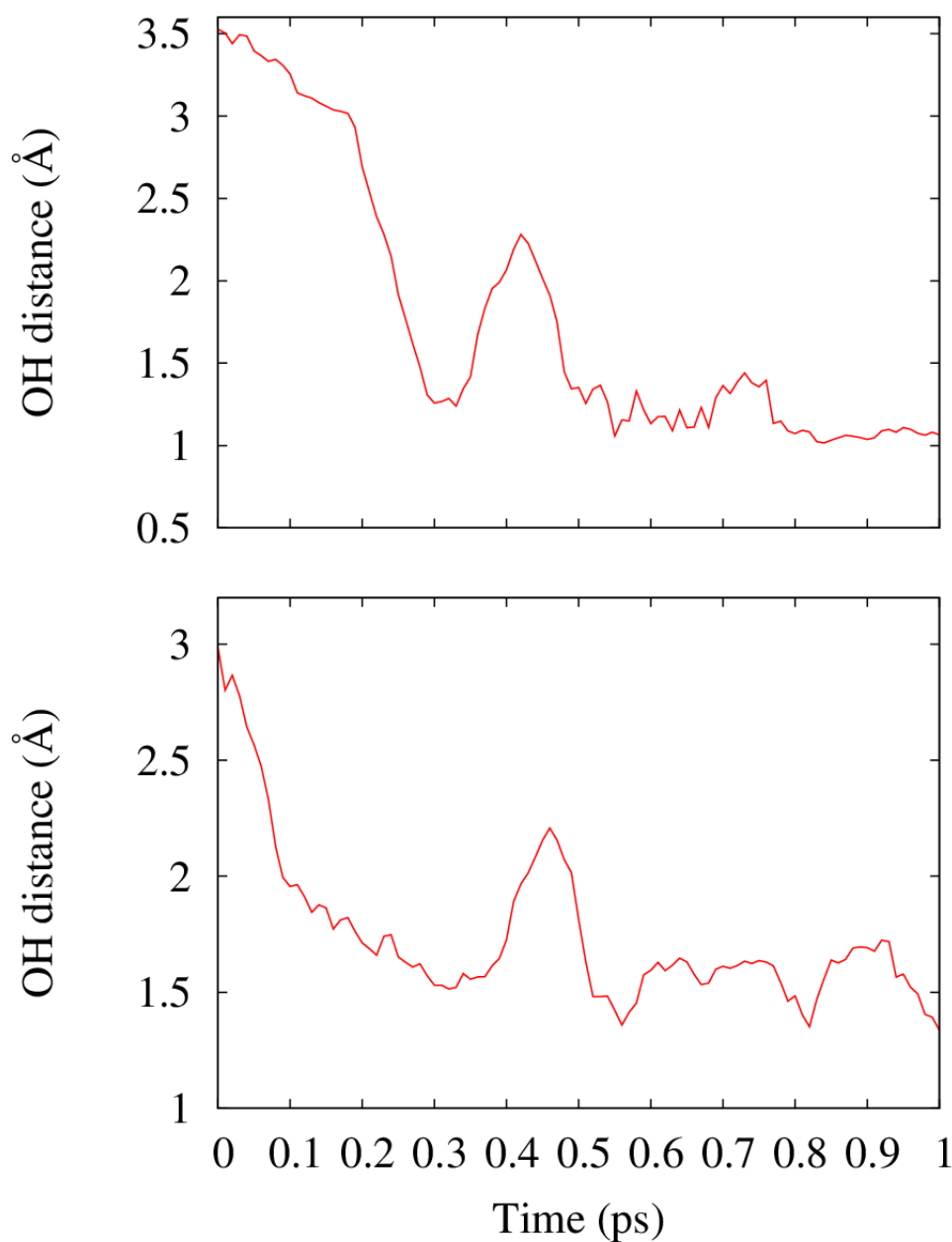
Figure 4: Evolution of various OH distances along a representative CPMD trajectory for configuration A1. Top: The distance between H(6) in H_2CO_3 and the nearest water oxygen. Bottom: The distance between O(2) in H_2CO_3 and the nearest water hydrogen. The atomic labels are defined in Figure 2.

Figure 5: Snapshots of the dissociation of H_2CO_3 from a representative CPMD trajectory starting in configuration A2. From left to right: 1. Hydrogen bond formation between the hydroxyl oxygen of H_2CO_3 and an adjacent water molecule ($t \approx 2.0$ ps) 2. Hydrogen bond formation between the carbonyl oxygen and an adjacent water molecule ($t \approx 3.0$ ps) 3. Formation of a Zundel-like structure ($t \approx 3.3$ ps) 4. Formation of a contact ion pair ($t \approx 3.5$ ps) 5. Complete dissociation takes place, yielding a solvent-separated ion pair ($t \approx 3.6$ ps).
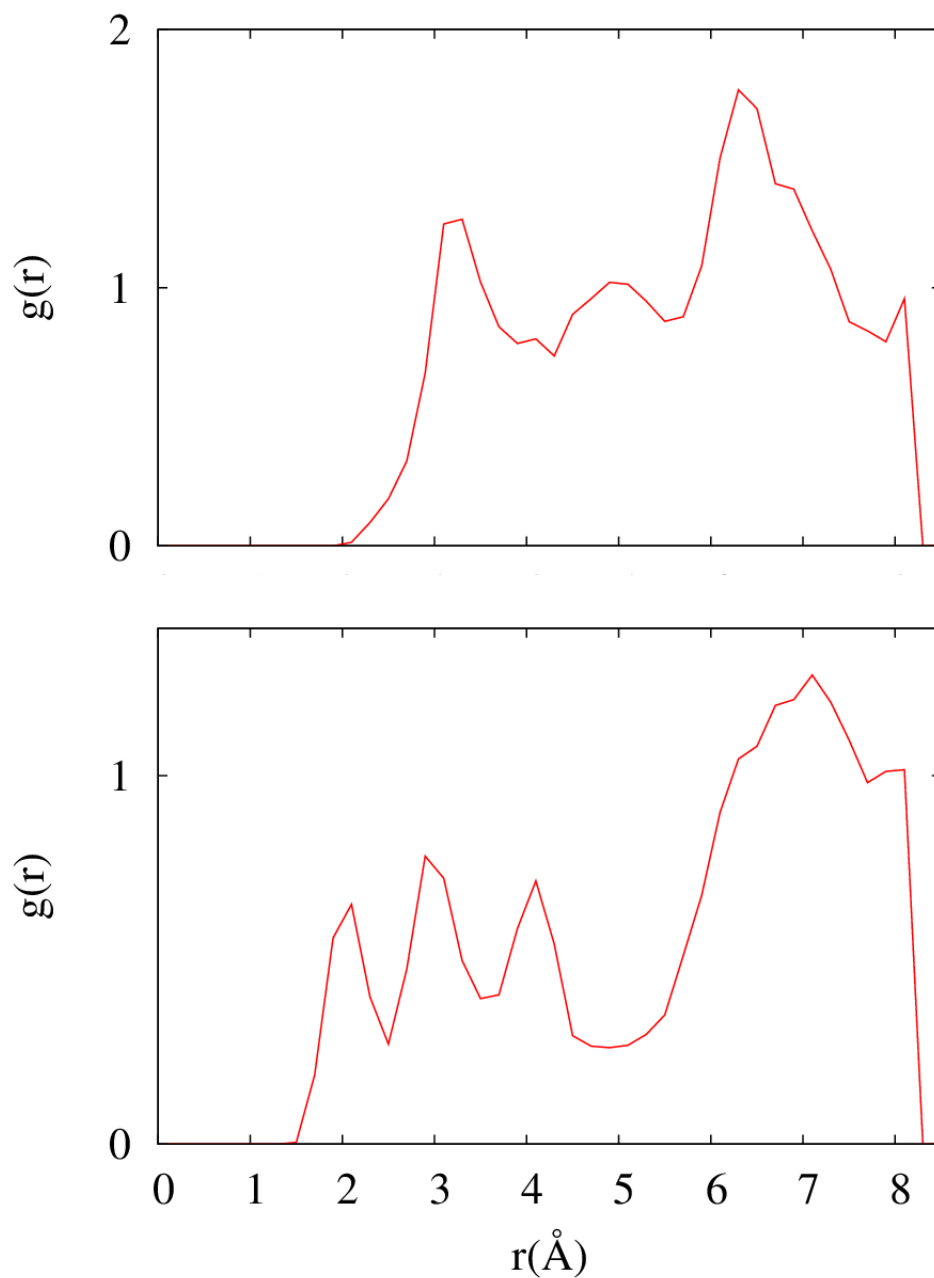
Figure 6: Snapshots of the dissociation of H_2CO_3 from a representative CPMD trajectory starting in configuration B1. From left to right: 1. Hydrogen bond formation between the hydroxyl oxygen in H_2CO_3 and an adjacent water molecule ($t \approx 0.5$ ps) 2. Second hydrogen bond formation between the same hydroxyl oxygen and another adjacent water molecule ($t \approx 2.0$ ps) 3. Formation of a Zundel-like structure ($t \approx 3.5$ ps) 4. Formation of a contact ion pair ($t \approx 4.0$ ps) 5. Complete dissociation takes place, yielding a solvent-separated ion pair ($t \approx 4.1$ ps).

Figure 7: H_2CO_3 oxygen [O(3)]−water hydrogen radial distribution functions for configurations B1 (top) and B2 (bottom). They were calculated by averaging data from the start of the production run until the dissociation takes place. The atomic labels are defined in Figure 2.
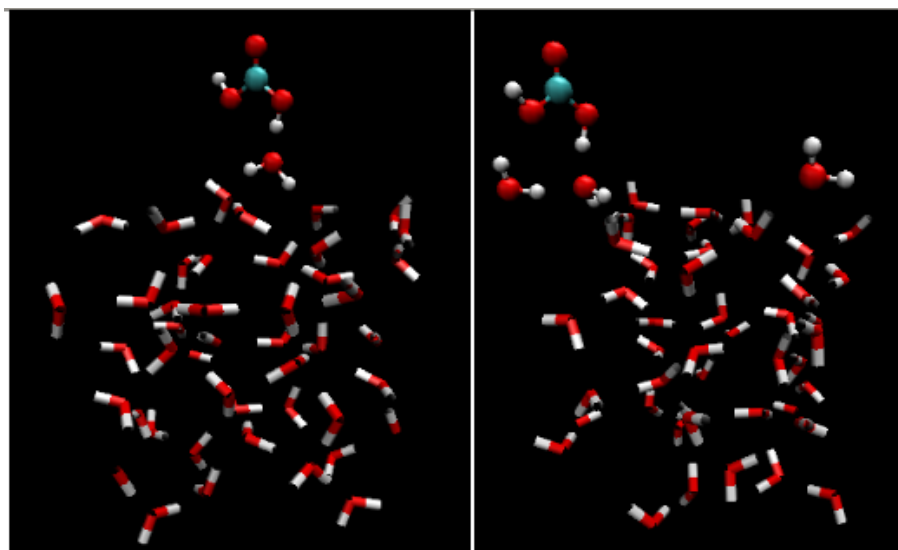
Figure 8: Snapshots of the hydrogen bond formation of H_2CO_3 from a representative CPMD trajectory starting in configuration B2. Left: Hydrogen bond formation between the hydroxyl oxygen in H_2CO_3 and an adjacent water molecule ($t \approx 1.0$ ps) Right: Formation of a weak hydrogen bond between the other hydroxyl oxygen in H_2CO_3 and another water molecule ($t \approx 2.0$ ps).
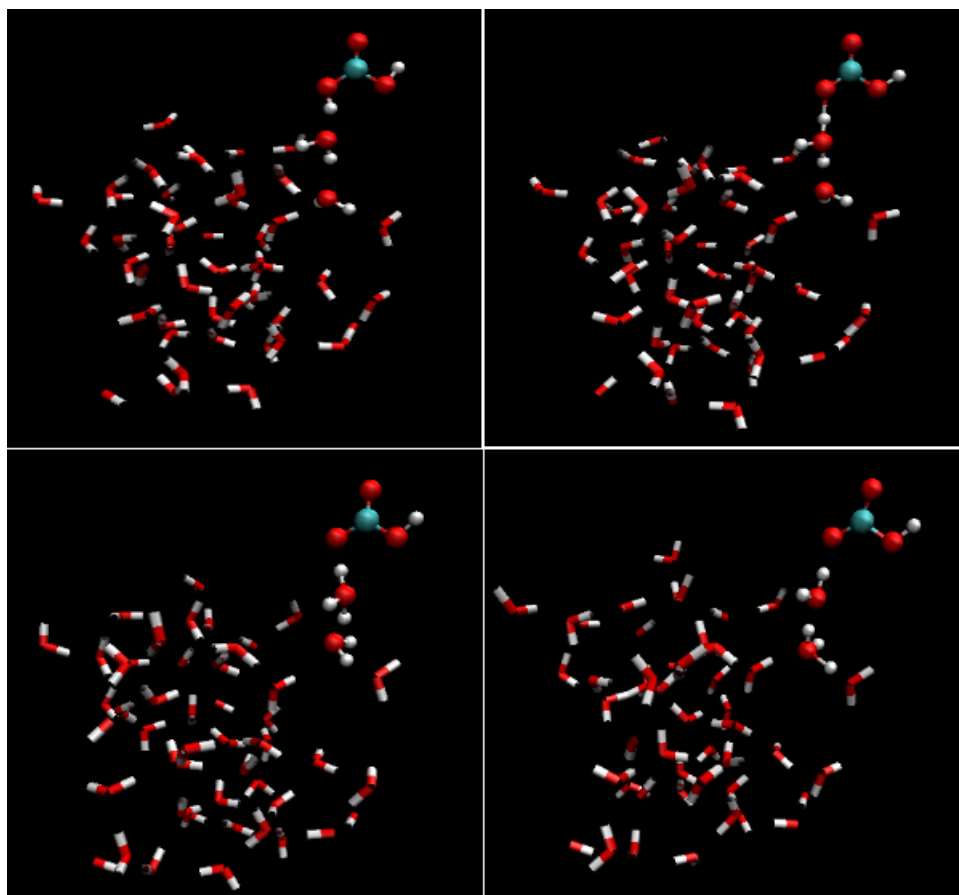
Figure 9: Snapshots of the dissociation of H_2CO_3 along a representative metadynamics trajectory for configuration B2. Top Left: Hydrogen bond formation between the donor oxygen in H_2CO_3 and the acceptor oxygen in an adjacent water molecule. Top right: Formation of a Zundel-like structure. Bottom left: Formation of a metastable contact ion pair. Bottom right: Complete dissociation takes place, yielding a solvent-separated ion pair.
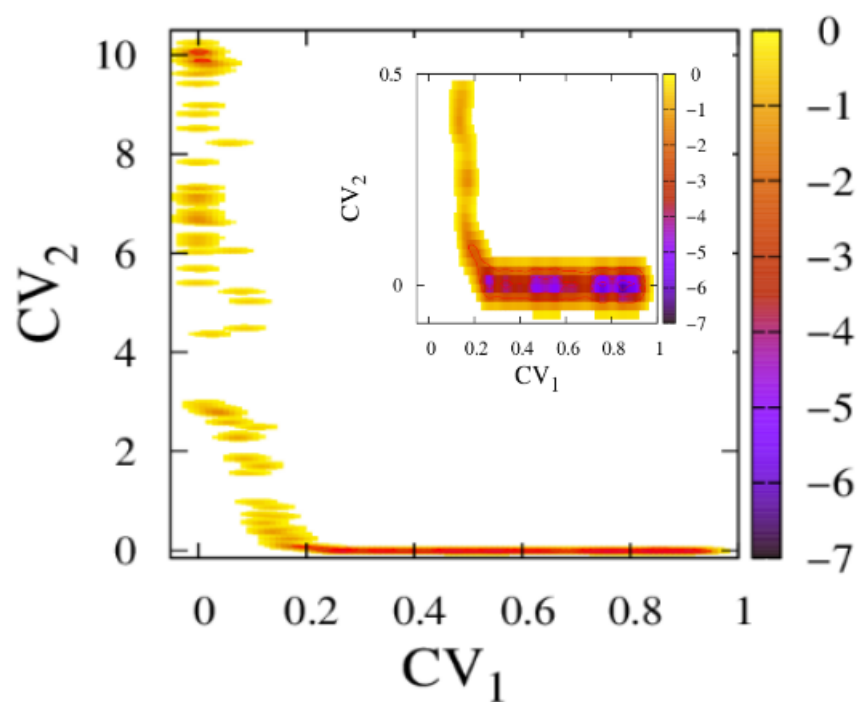
Figure 10: Free energy (in kcal/mol) profile as a function of CV_1 and CV_2 (in units of Bohr radius) for the dissociation of H_2CO_3 in configuration B2.
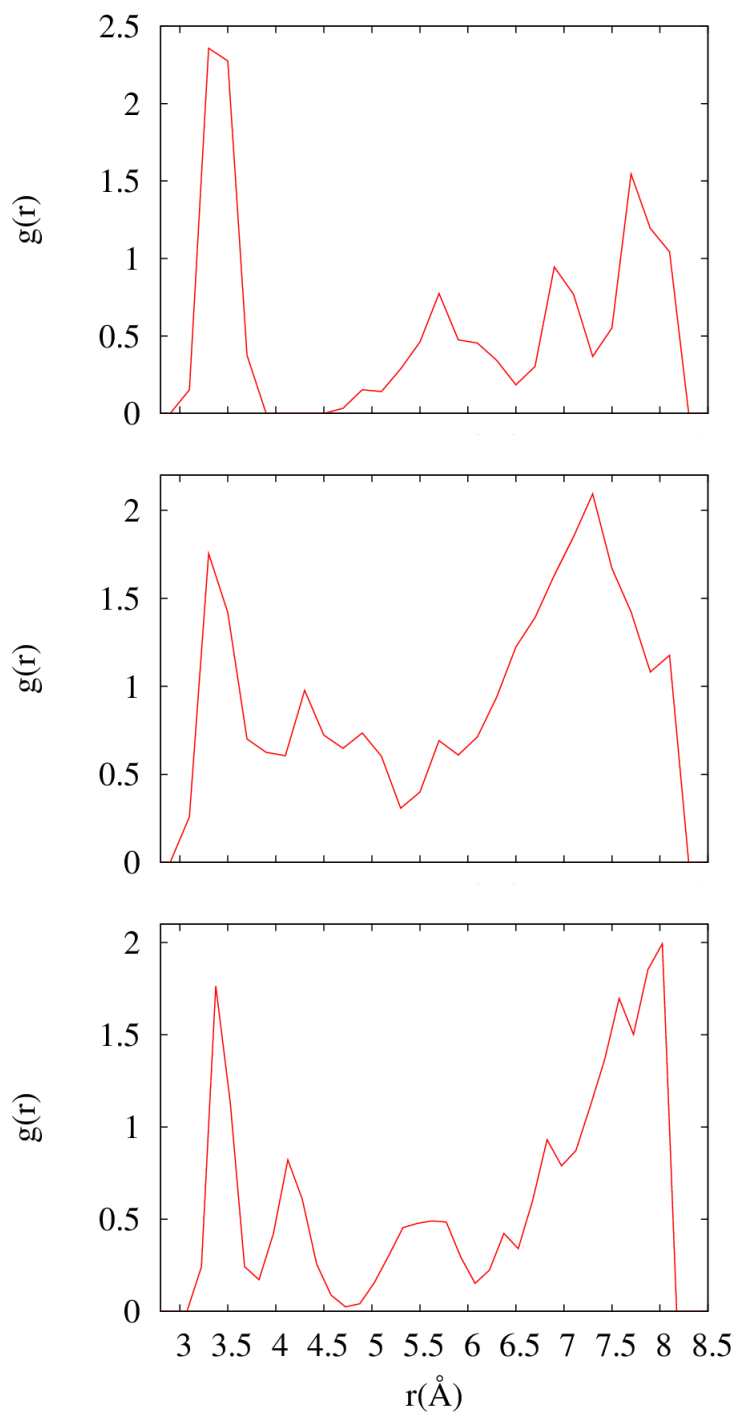
Figure 11: H_2CO_3 carbon$-$water oxygen radial distribution functions for configurations A2 (top), B1 (middle), and B2 (bottom).
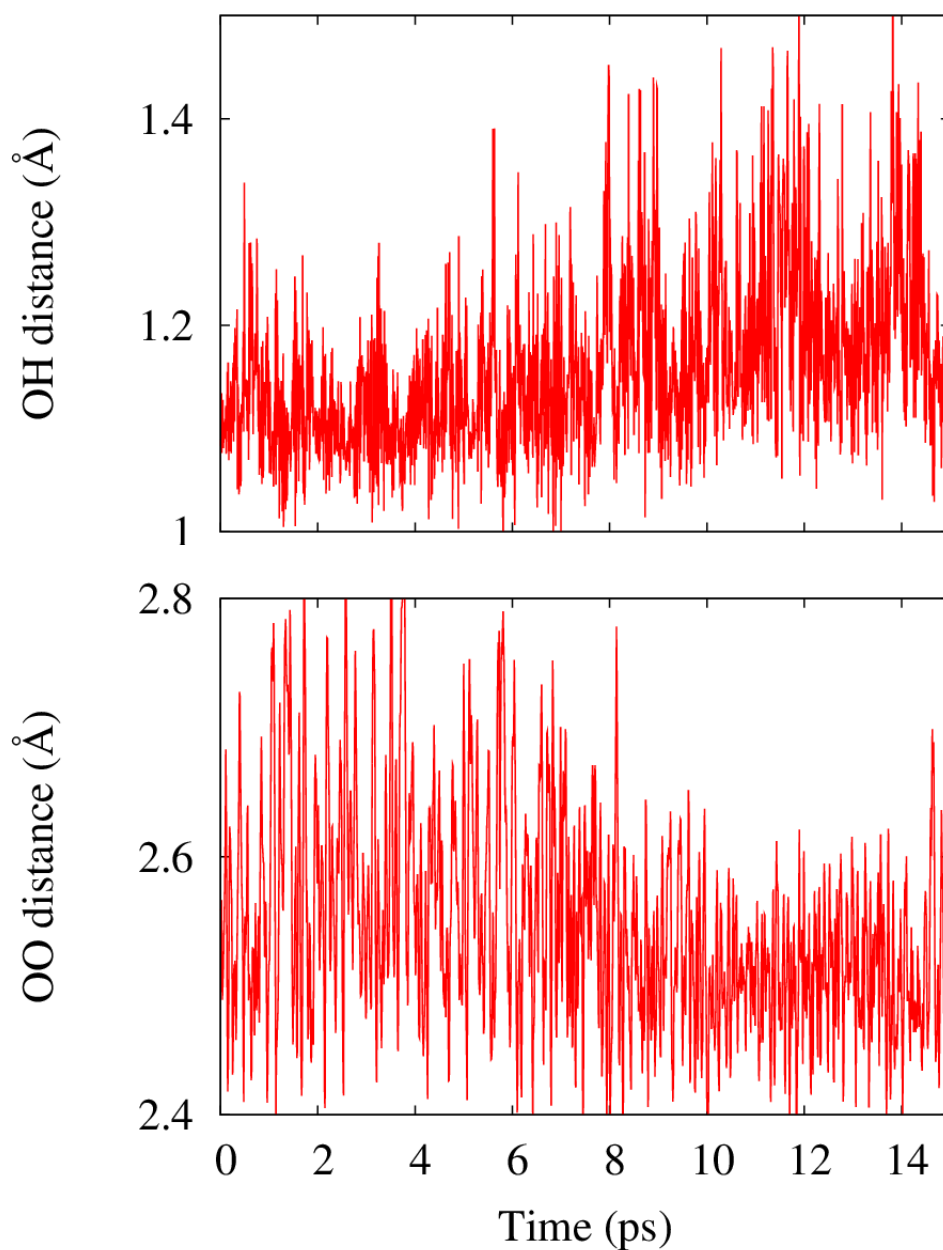
Figure 12: Evolution of various distances along a representative CPMD trajectory for configuration B2. Top: The distance between H(5) in H_2CO_3 and the nearest water oxygen. Bottom: The distance between O(4) in H_2CO_3 and the nearest water oxygen. The atomic labels are defined in Figure 2.
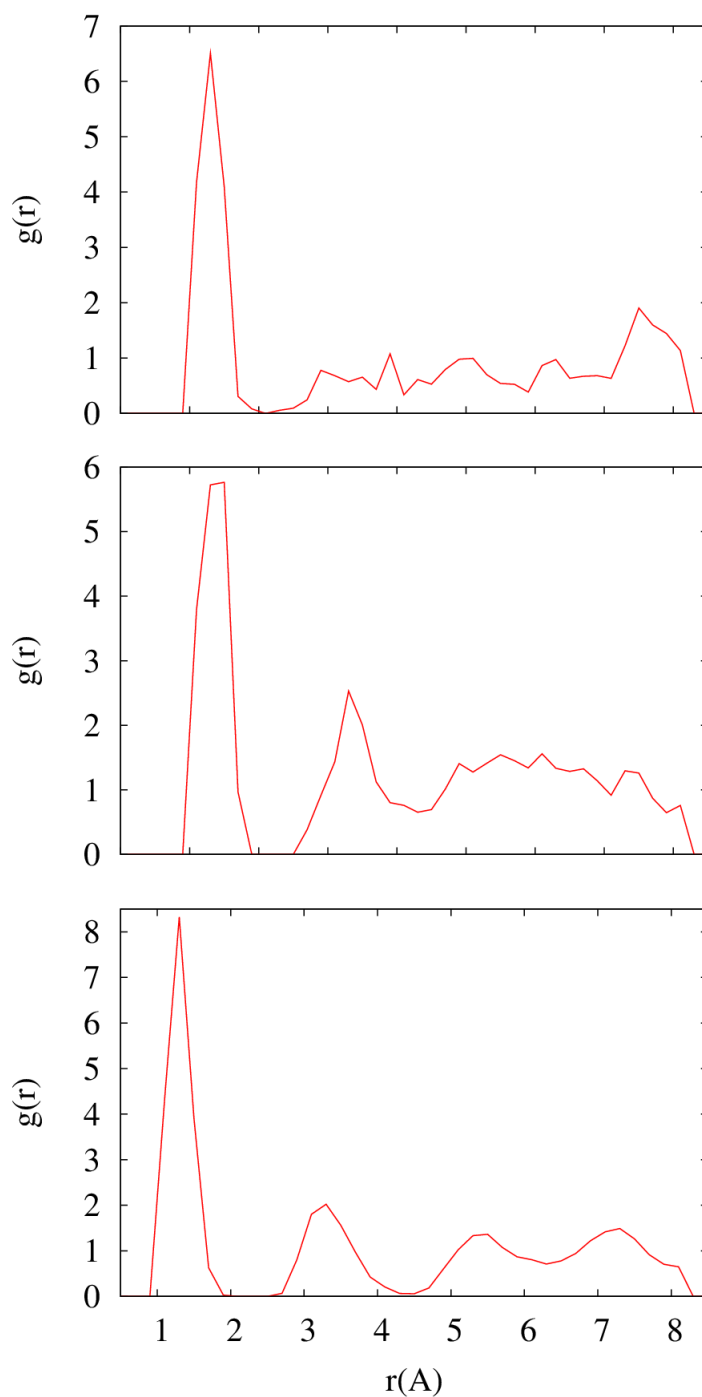
Figure 13: H_2CO_3 hydrogen [H(5) for A and H(6) for B]−water oxygen radial distribution functions for configurations A2 (top), B1 (middle), and B2 (bottom). They were calculated by averaging data from the start of the production run until the dissociation takes place. The atomic labels are defined in Figure 2.
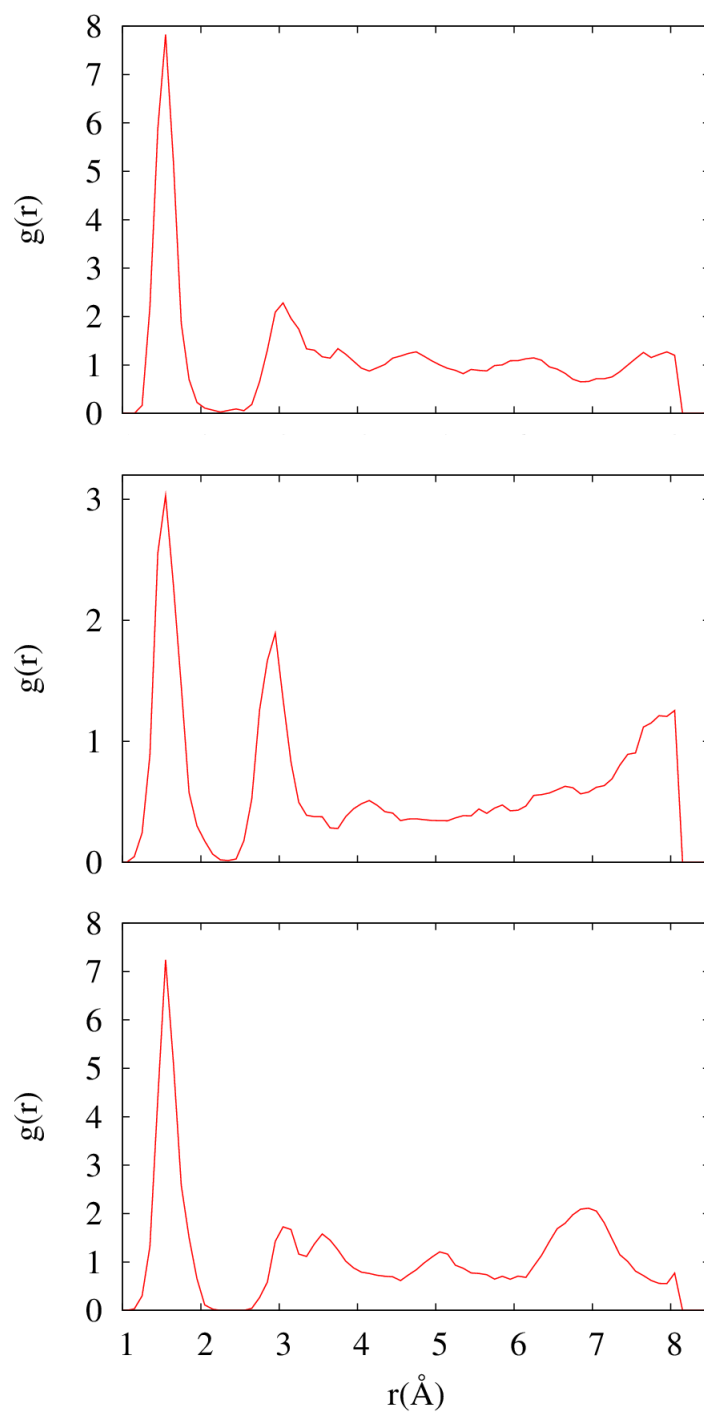
Figure 14: HCO_3^- oxygen [O(2) for A and O(4) for B]−water hydrogen radial distribution functions for configurations A1 (top), A2 (middle), and B1 (bottom). The atomic labels are defined in Figure 2.